Journal of Solid State Chemistry 183 (2010) 2759–2762

Contents lists available at ScienceDirect

Journal of Solid State Chemistry

journal homepage: www.elsevier.com/locate/jssc

Synthesis, crystal structure and nonlinear optical property of $Rb_3V_5O_{14}$

Jianguo Pan *, Yuebao Li, Yuejie Cui, Lingyan Zhao, Xing Li, Lei Han

State Key Laboratory Base of Novel Functional Materials and Preparation Science, Faculty of Materials Science and Engineering, Ningbo University, Ningbo, Zhejiang 315211, PR China

ARTICLE INFO

Article history:
Received 16 July 2010
Received in revised form
9 September 2010
Accepted 14 September 2010
Available online 18 September 2010

Keywords:
Crystal structure
Nonlinear optical material
$Rb_3V_5O_{14}$

ABSTRACT

The new nonlinear optical crystal $Rb_3V_5O_{14}$ has been synthesized by solid state reaction and characterized by single-crystal X-ray diffraction, IR and thermogravimetric analysis. The crystal $Rb_3V_5O_{14}$ crystallizes in the trigonal system with space $P31m$ (No. 157), $a=b=8.7134(12)$ Å, $c=5.2807(11)$ Å and $\alpha=90^\circ$, $\beta=90^\circ$, $\gamma=120^\circ$, $Z=1$, $\rho=3.516$ g/cm^3. It is a layered structure that is very flat and strongly parallel to c. The V_5O_{14} layer structure consists of corner-linked square and triangular pyramids. The layers are separated by Rb^+ ions, which fit equally well on the V_5O_{14} layer. The Kurtz powder SHG measurement, using 1064 nm radiation, showed that the second-harmonic generation efficiency of $Rb_3V_5O_{14}$ is about two times that of KDP.

1. Introduction

Nonlinear optical (NLO) crystals have wide applications in all solid-laser devices. During the past two decades, great progress has been made in searching for novel NLO crystals in inorganic oxides, organic crystals, polymers and organometallic compounds [1,2] for the use in ultraviolet and visible spectral regions. In general, vanadium may exist as V^0 (metallic), V^{2+}, V^{3+}, V^{4+} and V^{5+} depending on the synthesis procedure and chemical environment. Therefore, it can be the formation of many new structures, and has many interesting properties. Our interest in vanadium is based on its ability to form distorted tetrahedron, pentahedron, triangular pyramids, and octahedron. This type of distortion is prevalent in high-valent, d^0 transition metals owing to the symmetry-allowed mixing of a low-lying excited state (LUMO) with a nondegenerate ground-state molecular orbital (HOMO) [3–6]. This orbital mixing results in a distortion of the geometry of the metal centers along the $C2$, $C3$ or $C4$ axis whose magnitude is partially a function of the charge of the metal center, with increasing charge resulting in a smaller HOMO–LUMO gap [7–9]. Based on the above new crystal with large second-harmonic generation (SHG) responses can be prepared, such as $ACa_9(VO_4)_7$ [10], $Ba_{1.5}VOSi_2O_7$ [11], $K_3V_5O_{14}$ [12] and $A[(VO)_2(IO_3)_3O_2]$ (A=NH_4,Rb, Cs) [13], which are of interest as a result of their nonlinear optical properties as well as their piezoelectric and pyroelectric properties.

Howard et al. [14] report the crystal structure of $K_3V_5O_{14}$. The point group symmetry is ditrigonal pyramidal C_{3v}, the space group is $P31m$ (No. 157), $a=8.6899(6)$ Å, $c=5.0028(6)$ Å, $V=327.17(5)$ Å^3, $\rho=3.01$ g cm^{-3}. In this paper, we report the synthesis of $Rb_3V_5O_{14}$ crystal and some of its properties. $Rb_3V_5O_{14}$ and $K_3V_5O_{14}$ are isostructural, both bear a close resemblance to that of $K_3Ta_3B_2O_{12}$, which has a similar layered trigonal topology [15].

2. Experimental

2.1. Synthesis of $Rb_3V_5O_{14}$

$Rb_3V_5O_{14}$ were prepared by high-temperature solid-state reaction according to the following reactions:

$$3Rb_2CO_3+5V_2O_5 \rightarrow 2Rb_3V_5O_{14}+3CO_2\uparrow.$$

The stoichiometric amounts of Rb_2CO_3(AR) and V_2O_5(AR) were weighed accurately, where V_2O_5 was overweighed in order to compensate for volatilization of V_2O_5 during synthesis. According to many times experiments, it is appropriate that V_2O_5 was overweighed about 3%. These mixtures were pressed into tablets and then placed in platinum crucible. Platinum was selected since it is essentially chemically inert in this system. The samples were gradually heated to 500 °C for 15 h, held for 24 h and then allowed to cool to about 100 °C at a controlled temperature reducing rate of 1 °C/min in the furnace. The brown single crystals with dimension $5\times5\times2$ mm^3 were collected.

2.2. Structure determination

A typical single crystals of $Rb_3V_5O_{14}$ with dimensions of $0.23\times0.17\times0.15$ mm^3 were isolated from the crushed melted sample, and was mounted on a glass fiber for single crystal X-ray

* Corresponding author. Fax: +86 0574 87600734.
E-mail address: panjianguo@nbu.edu.cn (J. Pan).

0022-4596/$ - see front matter © 2010 Elsevier Inc. All rights reserved.
doi:10.1016/j.jssc.2010.09.017

diffraction analyses. Data collection of the complex was performed on a Rigaku R-AXIS RAPID three-circle diffractometer with graphite-monochromated Mo$K\alpha$ radiation ($\lambda=0.71073$ Å) at room temperature. All absorption corrections were applied using the SADABS program [16]. Cell refinement and data reduction were carried out with the use of the program SAINT in APEX II [17]. The structure was solved by the direct methods using program SHELXS and refined with the full-matrix least-squares by program SHELXL [18]. Additional experimental details are given in Table 1 and selected metrical details are presented in Tables 2–4.

2.3. Characterization

The XRD data of $Rb_3V_5O_{14}$ were collected at room temperature by Bruker D8 focus X-ray diffractometer with Cu$K\alpha$ radiation of wavelength $\lambda=1.5418$ Å in the scanning range of 2θ from 10° to 60°. The infrared spectrum in the region 400–4000 cm^{-1} was recorded at room temperature with a pressed KBr disk on a Nicolet 6700 infrared spectrophotometer. Thermal analysis was performed on PerkinElmer Pyris Diamond TG/DTA analyzer in N_2 atmosphere with a heating rate of 10 C/min. Powder SHG measurements were performed on a modified Kurtz-NLO system using a Q-switched and mode locked Nd:YAG laser with a wavelength of 1064 nm [19,20].

Table 1
Crystallographic data and structure refinement of $Rb_3V_5O_{14}$.

Formula	$Rb_3V_5O_{14}$
Space group	$P31m$
Crystal system	Trigonal
Formula units per cell/Z	1
Lattice parameters (Guinier powder data)	$a=b=8.7134(12)$ Å $c=5.2707(11)$ Å $\alpha=\beta=90°$ $\gamma=120°$ $V=347.21(10)$ Å^3
Molar mass (g mol^{-1})	735.11
Crystal size (μm^3)	$230\times170\times150$
ω range; increment	0–180°
Calculated density (g cm^{-3})	$\rho=3.516$ g/cm^3
Transmission (max/min)	0.499/0.271
Radiation	Mo$K\alpha$ ($\lambda=0.71073$ Å)
Absorption coefficient, μ (mm^{-1})	13.754
$F(000)$	338
θ-range [deg.]	3.86–27.43
Range in $h\ k\ l$	$\pm11\pm11\pm6$
Total reflections	3444
Independent reflections	3352
Data/parameters	565/3965/395/39
Goodness-of-fit	1.097
R indices [$I\geq2\sigma(I)$]	$R1=0.0613$ $WR2=0.1485$
R indices (all data)	$R1=.0568$ $WR2=0.1503$
Largest diff. peak and hole [e/Å^3]	1.25 − 1.47

$R_1(F)=\sum||F_o|-|F_c||/\sum|F_o|$.
$wR_2(F2)=\left[\sum w(F_o{}^2-F_c{}^2)^2/\sum w(F_o{}^2)^2\right]^{1/2}$, $w=1/[\sigma^2(F_o^2)+(0.1200P)^2+18.3337P]$, $P=(F_o^2+2F_c^2)/3$.

Table 2
Selected interatomic distances (Å)for $Rb_3V_5O_{14}$.

Atoms	Distance (Å)	Atoms	Distance (Å)
Rb–O(3) × 2	2.923(6)	V(1)–O(2)	1.597(14)
Rb–O(1) × 2	3.004(8)	V(1)–O(4) × 2	1.813(8)
Rb–O(1) × 2	3.109(7)	V(1)–O(1) × 2	1.914(8)
Rb–O(2) × 2	3.165(5)	V(2)–O(3)	1.609(17)
Rb–O(2)	3.315(16)	V(2)–O(1) × 3	1.751(8)
Rb–O(4)	3.490(8)		

Table 3
Selected interatomic angles (deg.) for $Rb_3V_5O_{14}$.

Atoms	Angle	Atoms	Angle
O(1)–V(1)–O(1)	83.7(4)	O(2)–V(1)–O(1) × 2	105.1(5)
O(4)–V(1)–O(4)	88.0(4)	O(4)–V(1)–O(1) × 2	152.4(5)
O(2)–V(1)–O(4) × 2	102.4(5)	O(3)–V(2)–O(1) × 3	110.1(3)
O(4)–V(1)–O(1) × 2	87.7(4)	O(1)–V(2)–O(1) × 3	108.9(3)

Table 4
Refined fractional co-ordinates of $Rb_3V_5O_{14}$.

Atom	Wyck	x	y	z
Rb1	3c	0	0.38780(17)	0.1756(3)
V1	3c	−0.2306(3)	0	0.6690(5)
V2	2b	1/3	2/3	0.6580(5)
O1	6d	0.1692(10)	0.7088(9)	0.5443(16)
O4	3c	0.000(1)	0.1669(9)	0.6243(16)
O2	3c	−0.2529(18)	0	0.969(3)
O3	2b	1/3	2/3	0.963(3)

3. Results and discussion

3.1. Structure description

The structure of $Rb_3V_5O_{14}$ bears a closer resemblance to that of $K_3Ta_3B_2O_{12}$, which has a similar layered topology.

Two-dimensional layer separated by Rb^+ cations is depicted in Fig. 1. The layer character of this structure is very flat and strongly parallel to c. The $[V_5O_{14}]_n$ layer structure consists of corner-linked square and triangular pyramids. The five vanadium atoms lie very nearly in the same z-plane forming almost regular pentagons. The 14 oxygen atoms are bound to the vanadium atoms in an unusual way. As will be seen, the V_1 atoms form five bonds, one with O_2 atoms, two with O_4 and two with O_1 atoms, but the V_2 atoms form four bonds, one with O_3 atoms and three with O_1 atoms. They form nearly square pyramids around the V_1 atoms and trigonal pyramids around the V_2 atoms, the pyramids all with apices pointing in the same direction along the c-axis and joined by sharing neighboring basal corners. Each hollow space resulting from the five-ring configuration is occupied by a rubidium atom, placed about half way between the layers. Each rubidium is surrounded by 10 oxygen's, five from the apex oxygen's of the polyhedra in the lower layer and five from basal corner of polyhedra in the layer above. The layers are separated by Rb^+ ions, which fit equally well on the V_5O_{14} layer. This packing mode is favorable to the accumulation of microscopic second-order NLO coefficient and hence exhibits a relatively strong bulk NLO effect.

3.2. X-ray diffraction analysis

The X-ray powder diffraction analysis was used to confirm the physical phase and purity of the product. Single crystal data were employed to simulate the powder pattern. The pattern is shown in Fig. 2. We can see that the powder pattern of the multicrystal matches that of the $Rb_3V_5O_{14}$ standard (PDF no. 36-1214) and that of single crystal simulation. But the diffraction intensity has some difference compared to the indexed and simulation pattern due to many factors such as the size of powder particulate, the control of

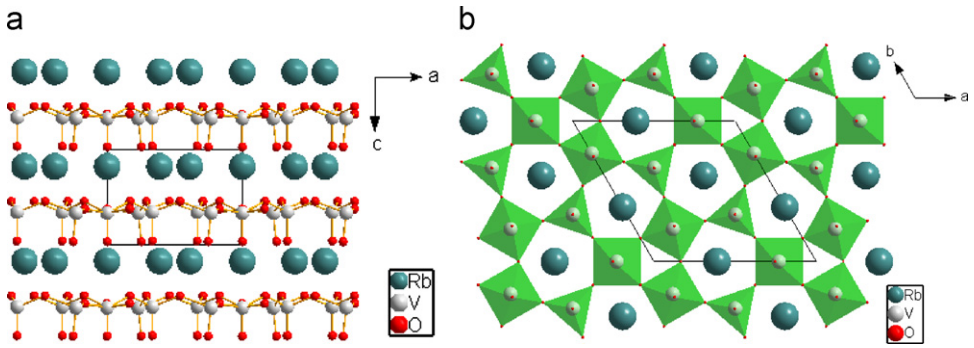

Fig. 1. View of the structure of $Rb_3V_5O_{14}$, corner-connected VO_4 triangular pyramids and VO_5 square pyramids interspersed with layers Rb ions (the green balls) is shown in projection down the [010] direction in (a) and the [001] direction in (b).

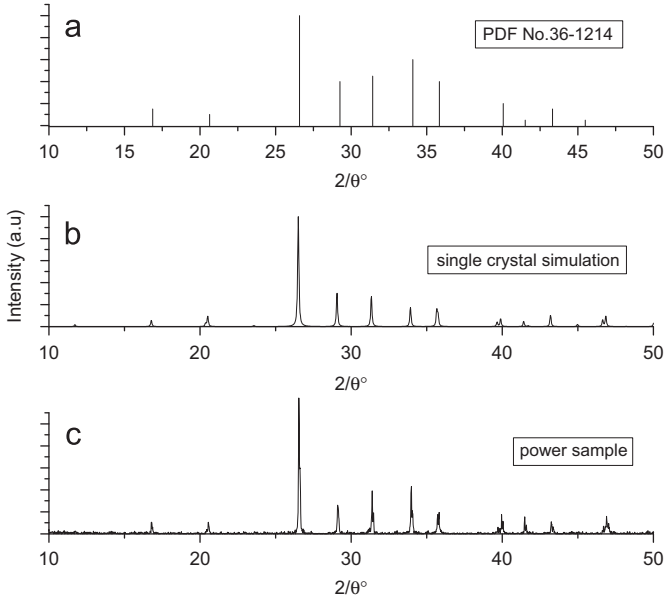

Fig. 2. The pattern of X-ray powder diffraction: (a) the indexed pattern, (b) single crystal simulation pattern and (c) powder sample pattern.

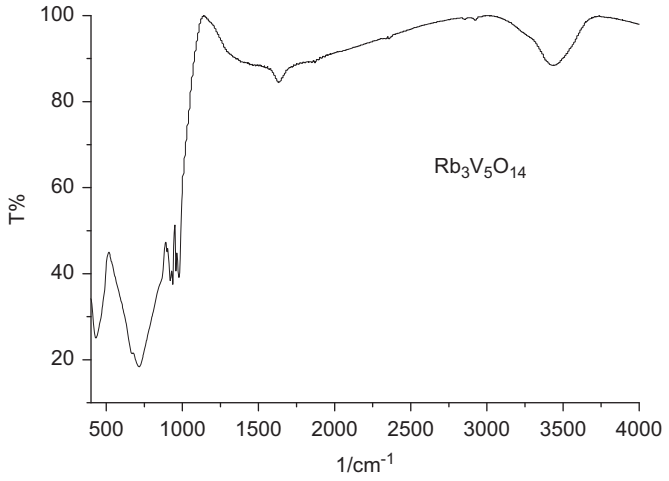

Fig. 3. IR spectrum of $Rb_3V_5O_{14}$ crystal.

the scanning conditions and the crystalline degree. Because of crystal defect and lattice deformation, there are some double peaks on the experimental pattern that are not founded on the PDF file.

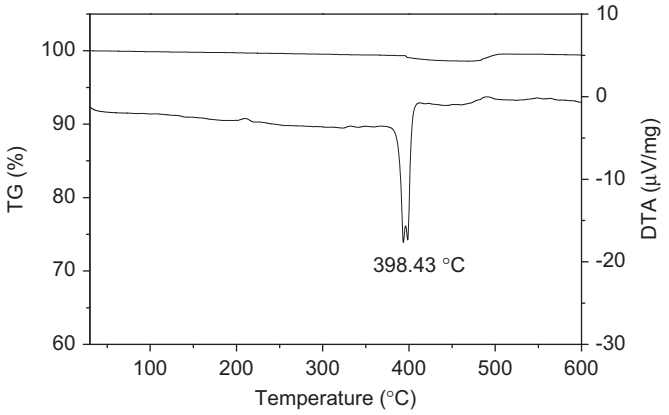

Fig. 4. TG and DTA curves of $Rb_3V_5O_{14}$ crystal.

3.3. Infrared spectrum and thermal studies

In $Rb_3V_5O_{14}$, there are VO_5 square pyramids and VO_4 trigonal pyramids. Each vanadium atom is displaced from the center of the polyhedron, resulting in on short V–O bond. The short bond is typical of V=O vanadyl group, involving both π and σ bonding. As shown in Table 2, there are two short V=O bonds (length of 1.597 Å in VO_5 square pyramids, length of 1.609 Å in VO_4 trigonal pyramids) and seven long V–O bonds (length of 1.823 Å, 1.914 Å in VO_5 square, length of 1.751 Å in VO_4 tetrahedron) in $Rb_3V_5O_{14}$. In $Cs_2VOP_2O_4$, $Rb_2(VO)_3(P_2O_7)_2$ infrared spectrum, the symmetric stretching vibrations of V=O bond appear near 900–980 cm^{-1}, and that of long V–O bond appear near 600–700 cm^{-1} [21]. The infrared spectrum of the $Rb_3V_5O_{14}$ crystalline powder was shown in Fig. 3. With short V=O length 1.597 and 1.609 Å, the symmetric stretching vibrations of the V=O is observed at 978 and 934 cm^{-1}. The symmetric stretching vibrations of the longer V–O bonds appear in region 650–720 cm^{-1}. The 3430 and 1640 cm^{-1} peaks may be assigned to the O–H stretching and bending vibrations, they are indicative of the moisture regain of $Rb_3V_5O_{14}$. We can confirm that the main transparent range of $Rb_3V_5O_{14}$ in IR region is 1000–4000 cm^{-1}. The TG and DTA curves of $Rb_3V_5O_{14}$ crystal are shown in Fig. 4. From the TG and DTA curves it is observed that, there is no weight loss at temperatures below 600 °C. The melting point of the $Rb_3V_5O_{14}$ crystal is about 398 °C, which shows that $Rb_3V_5O_{14}$ crystal is congruently melt.

3.4. Nonlinear optical properties

A preliminary SHG efficiency measurement of $Rb_3V_5O_{14}$ has been carried out by the Kurtz–Perry method using polycrystalline

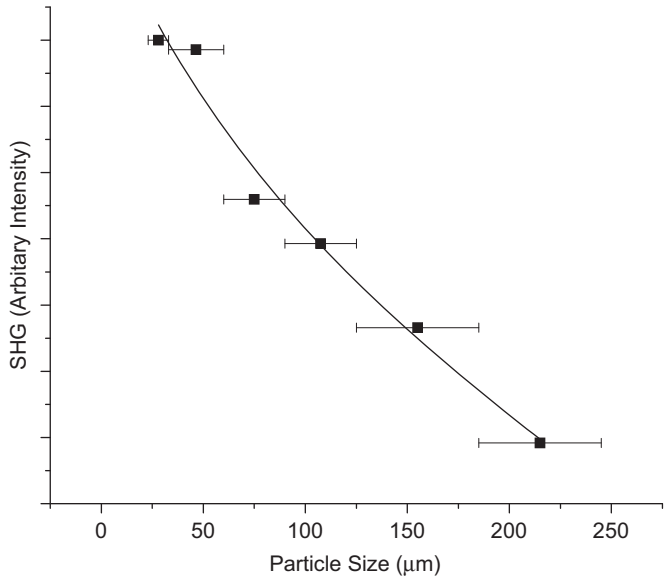

Fig. 5. Phase-matching, i.e., particle size vs. SHG intensity, data for $Rb_3V_5O_{14}$.

samples at room temperature. In addition to identifying the materials with noncentrosymmetric crystal structure, it is also used as a screening technique to identify the materials with the capacity for phase matching. The SHG intensity from the material is measured as a function of particle size. The continuous increase of SHG intensity with increase in particle size and remaining essentially constant at particle sizes greater than the coherence length confirms the phase matching behavior of the material [22].

With the 100 μm particle size, the intensity of the green light (frequency-doubled output: $\lambda=532$ nm) produced by the $Rb_3V_5O_{14}$ powder is about two times that of KDP powder, indicating that $Rb_3V_5O_{14}$ is two times the SHG efficiency of KDP. Fig. 5 shows the curves of SHG signal as a function of particle size, which are not consistent with phase-matching behavior. The continuous increase of SHG with decrease in particle size [19,23] shows that $Rb_3V_5O_{14}$ crystal is of non-phase matching behavior.

4. Conclusions

A novel second-order NLO material of Rubidium pentavanadium was synthesized by high-temperature solid-state reaction. Its single crystal with the size of $5\times5\times2$ mm^3 has been grown by cooling melts of Rb_2CO_3 and V_2O_5. The crystal $Rb_3V_5O_{14}$ crystallizes in the trigonal system with space $P31m$ (No. 157), $a=b=8.7134(12)$ Å, $c=5.2807(11)$ Å and $\alpha=90^\circ$, $\beta=90^\circ$, $\gamma=120^\circ$, $Z=1$, $\rho=3.516$ g/cm^3. It is a layered structure that is very flat and strongly parallel to c. The intensity of second harmonic generation effect is about 2 times as large as that of KDP. The $Rb_3V_5O_{14}$ crystal is transparent in most of IR region, and the transparent range is 1000–4000 cm^{-1}. The melting point of $Rb_3V_5O_{14}$ is about 398 °C. It is possible for $Rb_3V_5O_{14}$ to possess potential application as a new NLO crystal in IR region.

During the revision process of this paper, the synthesis and structure of $Rb_3V_5O_{14}$ has been reported in the literature [24].

Acknowledgments

This work is partially supported by the National Natural Science Foundation of China (No. 61078055), Ningbo Municipal Natural Science Foundation (No. 2009A610015), the Program for Innovative Research Team of Ningbo Novel Photoelectric Materials and Devices (2009B21007) and the K.C. Wang magna Fund in Ningbo University.

Appendix A. Supplementary material

Supplementary data associated with this article can be found in the online version at doi:10.1016/j.jssc.2010.09.017.

References

[1] P. Becker, Adv. Mater. 10 (1998) 979–992.
[2] X.Y. Fan, R.C. Eckardt, R.L. Byer, C. Chen, IEEE J. Quantum Electron. 25 (1989) 1196–1199.
[3] R.A Wheeler, M.H Whangbo, T. Hughbanks, R Hoffman, J.K Burdett, T.A. Albright, J. Am. Chem. Soc. 108 (1986) 2222–2236.
[4] R.G. Pearson, J. Mol. Struct. 103 (1983) 25–34.
[5] S.K. Kang, H. Tang, T.A. Albright, J. Am. Chem. Soc. 115 (1993) 1971–1981.
[6] R.E. Cohen, Nature 358 (1992) 136–138.
[7] M. Kunz, I.D. Brown, J. Solid State Chem. 115 (1995) 395–406.
[8] J.B. Goodenough, J.M. Longo, in: K.H. Hellwege, A.M. Hellwege (Eds.), Landolt–Bornstein, 4, Springer-Verlag, Berlin, 1970, p. 126.
[9] I.D. Brown, Acta Crystallogr. B 33 (1977) 1305–1310.
[10] J.S.O. Evans, J. Huang, A.W. Sleight, J. Solid State Chem. 157 (2001) 255–260.
[11] K. Ramesha, J. Gopalakrishnan, Solid State Sci. 3 (2001) 113–119.
[12] G. Li, G. Su, X. Zhuang, Z. Li, Y. He, Opt. Mater. 27 (2004) 539–542.
[13] R.E. Sykora, K.M. Ok, P.S. Halasyamani, D.M. Wells, T.E. Albrecht-Schmitt, Chem. Mater. 14 (2002) 2741–2749.
[14] T. Howard, H. Evans Jr., A.M. Brusewitz, Acta Chem. Scand. 48 (1994) 533–536.
[15] J. Choisnet, D. Groult, B. Raveau, M. Gasprain, Acta Crystallogr. B 33 (1977) 1841–1845.
[16] Bruker, SMART Version 5.054 Data Collection and SAINT-Plus, Version 6.45a Data Processing Software for the SMART System, Bruker Analytical X-ray Instruments, Inc., Madison, WI, USA, 2003.
[17] Bruker, APEX2 Version 2.1-4 and SAINT Version 7.23a Data Collection and Processing Software, Bruker Analytical X-ray Instruments, Inc., Madison, WI, USA, 2006.
[18] G.M. Sheldrick, Acta Crystallogr. A Found. Crystallogr 64 (2008) 112–122.
[19] S.Q. Kurtz, T.T. Perry, J. Appl. Phys. 39 (1968) 3798–3813.
[20] Y. Porter, K.M. Ok, N.S.P. Bhuvanesh, P.S. Halasyamani, Chem. Mater. 13 (2001) 1910–1915.
[21] V.P. Mahadevan. Pillai, B.R. Thomas, V.U. Nayar, K.H. Lii, Spectrochim. Acta Part A 55 (1999) 1809–1817.
[22] A. Sonoc, M. Samoc, P.N. Prasad, J. Opt. Soc. B9 (1992) 1819–1824.
[23] J.P. Dougherty, S.K. Kurtz, J. Appl. Crystallogr. 9 (1976) 145–158.
[24] J Yeon, S.H. Kim, P.S. Halasyamani, Inorg. Chem. 49 (2010) 6986–6993.